Korean J. Chem. Eng., 38(11), 2247-2255 (2021)
DOI: 10.1007/s11814-021-0853-x

pISSN: 0256-1115
eISSN: 1975-7220

Fabrication and modification of cellulose aerogels from Vietnamese water hyacinth for oil adsorption application

La Nam Phat[*,], Tran Quoc Thang[***], Huynh Cam Nguyen[*,**], Dang Thi My Duyen[*,**], Dao Xuan Tien[***], Bui Dang Dang Khoa[*,**], Pham Tan Khang[*,**], Nguyen Thi Huong Giang[*,**], Hoang Minh Nam[*,**,****], Mai Thanh Phong[*,**,****], and Nguyen Huu Hieu[*,**,****,†]**

*VNU-HCM, Key Laboratory of Chemical Engineering and Petroleum Processing (Key CEPP Lab), Ho Chi Minh City University of Technology (HCMUT), 268 Ly Thuong Kiet Street, District 10, Ho Chi Minh City, Vietnam
**Faculty of Chemical Engineering, Ho Chi Minh City University of Technology (HCMUT), 268 Ly Thuong Kiet Street, District 10, Ho Chi Minh City, Vietnam
***Faculty of Chemistry Ho Chi Minh City University of Science (HCMUS), 227 Nguyen Van Cu Street, District 5, Ho Chi Minh City, Vietnam
****Vietnam National University Ho Chi Minh City, Linh Trung Ward, Thu Duc District, Ho Chi Minh City, Vietnam
(*Received 24 March 2021 • Revised 15 May 2021 • Accepted 20 May 2021*)

Abstract−Recycling biomass to cellulose aerogel (Cell-A) provides a promising approach to develop adsorbent materials for spilled-oil recovery. In this work, Cell-A was fabricated from Vietnamese water hyacinth via crosslinking methods using PVA as a crosslinker and freeze-drying process. Various cellulose to PVA ratios were investigated to obtain the optimal synthesis condition. The Cell-A was additionally modified by dip-coating in poly(dimethylsiloxane) (PDMS) and pyrolyzing to form PDMS-coated cellulose aerogels (Cell-AP) and carbon aerogels (CA), respectively. Results of the oil adsorption tests show that pyrolysis produced aerogels with greater adsorption capacity with an optimal mass ratio of 15 : 1 cellulose to PVA. Furthermore, the pseudo-second-order model was found to be more accurate than the pseudo-first-order model for the study of oil absorption kinetics. As a result, the modified cellulose aerogel is promising for replacing earth-unfriendly polymer-based oil sorbents due to their high oil absorption capacity.

Keywords: Oil-spill Cleaning, Oil Adsorbent, Aerogel Materials, Biomass Recycling

INTRODUCTION

Petroleum contamination is a major environmental concern due to its harm to both terrestrial and aquatic ecosystems. The contamination of marine habitats, in particular, has caught the attention of researchers and environmentalists due to its serious impact on marine life and on people whose livelihood depends on the sea's resources. In 1989, the Exxon Valdez spilled 37,000 tons of oil into the Prince William Sound on the south of Alaska, USA, killing a total of 35,467 seabirds [1]. Various solutions to this issue have been searched for in recent decades, including chemical oxidation, adsorption, membrane separation, and treatment. Among these, adsorption is considered one of the most effective due to ease of operation, low cost, non-toxicity, and large capacity. The performance of aerogels as an oil adsorbent and production from Vietnamese water hyacinth, in particular, are subjects of current interest.

Aerogel, a porous material with a three-dimensional structure obtained from the process of exchanging the liquid solvent with air, is used in optoelectronics, catalyst support, soundproofing, thermal insulation, energy storage devices, adsorbents, and many other applications [2]. Cellulose aerogel (Cell-A) synthesized from cellulose fibers has a unique structure and properties involving its 3D network structure, an ultra-low density (0.016-0.112 g/cm^3), immensely high porosity (91.9-98.9%), extremely low thermal conductivity (0.031-0.042 W/mK), and high compressive strength (88 kPa) according to Young's modulus [3]. Cell-A is an eco-friendly and multifunctional material with diverse applications, e.g., adsorption and oil/water separation, thermal insulation, biomedical materials, and metal nanoparticles/metal oxide carriers [4]. Water hyacinth is a free-floating tropical perennial plant; it is considered an invasive species in many countries for multiple reasons, including its rapid rate of reproduction, adverse effects on freshwater ecosystems, river traffic and agriculture, hydropower and water supply systems, urban and surrounding environment view. To curb its growth, different management strategies, such as physical, chemical, biological, and integrated methods, have been used. Noticing the rapid spread of water hyacinths in Vietnam, as proposed by the Department of Transportation of the city, the People's Committee of Ho Chi Minh city spent approximately 30 billion VND on removing water hyacinth in all canals [5]. Despite its severe impact on infested regions, water hyacinth has a wide range of practical applications; particularly, it is one of the aquatic plant species successfully used for water treatment. Although it is efficient in removing water pollutants like organic matter, heavy metals ions, and pathogens, its adsorption applications are limited and have not been studied widely [6]. Its high cellulose content and low lignin content suggest that water hyacinth

†To whom correspondence should be addressed.
E-mail: nhhieubk@hcmut.edu.vn

Table 1. Ratio of cellulose to PVA

Samples	Cellulose : PVA (g : g)				
	5 : 1	10 : 1	15 : 1	20 : 1	25 : 1
Cellulose aerogel	Cell-A05	Cell-A10	Cell-A15	Cell-A20	Cell-A25
PDMS modified	Cell-AP05	Cell-AP10	Cell-AP15	Cell-AP20	Cell-AP25
Pyrolyzed	CA-05	CA-10	CA-15	CA-20	CA-25
pH			Neutral		

can be used as a source of material to synthesize Cell-A for oil adsorption applications. This could potentially be a solution to Vietnam's water hyacinth infection [7].

We fabricated Cell-A from Vietnamese water hyacinth via cross-linking method with PVA as a cross-linker and a freeze-drying process [8]. PVA can create a solid structure for the gel network [9]. Besides, PVA is a reasonably affordable polymer which exhibits favorable characteristics, such as biodegradability, biocompatibility, and water solubility [10]. The optimal synthesis condition was obtained through investigating various cellulose to PVA ratios. To achieve hydrophobicity and improve oil adsorption selectivity, Cell-A was then either surface-modified with poly(dimethylsiloxane) (PDMS) via dip-coating to obtain modified PDMS cellulose aerogel (Cell-AP) or pyrolyzed to produce carbon aerogel (CA). Characterization of Cell-A, Cell-AP, and CA was performed via their density and porosity, scanning electron microscopy (SEM), Fourier transform infrared spectroscopy (FTIR), X-ray diffraction (XRD), thermogravimetric analysis (TGA), Brunauer-Emmett-Teller (BET) specific surface area, and nitrogen adsorption/desorption. The hydrophobicity and oil adsorption of Cell-AP and CA were investigated via the water contact angle (WCA) and kinetics models, including the pseudo-first and pseudo-second-order models, respectively.

EXPERIMENTAL

1. Materials and Chemicals

Water hyacinth was collected from Thanh Da river, Ho Chi Minh City. Sodium hydroxide (NaOH), hydrogen peroxide (H_2O_2), acetic acid (CH_3COOH), formic acid (HCOOH), poly(vinyl alcohol) (PVA), and hexane (C_6H_{14}) were all of the analytical grades and purchased from Xilong Scientific. Dibutyltin dilaurate (DBTL), tetraethyl orthosilicate (TEOS), and poly(dimethylsiloxane) (PDMS) were provided by Sigma-Aldrich, Macklin, and Acros Organic, respectively. Used lubricating oil (Shell Advanced 20w50) was collected from Saigon Petro and all the solutions were prepared with deionized water.

2. Preparation of Cellulose from Water Hyacinth

Water hyacinth was soaked in a 1 M NaOH solution in a ratio of 1 : 40 (g : mL) at 80 °C for 2 hours, followed by washing with deionized water to remove residual impurities and adjusting pH from 11 to 7. To obtain purified cellulose, 30% H_2O_2 solution was infused with a mixture of 3 : 7 volume ratio of acetic acid to formic acid. Pretreated water hyacinth was immersed in the above liquid mixture at a ratio of 1 : 6 (g : mL) at 90 °C for 3 hours. The obtained acidic water hyacinth pulp was washed and adjusted to neutral pH before being dried at 90 °C in a drying oven.

3. Preparation of Cell-A

Various amounts of pretreated cellulose were dispersed in aqueous PVA solutions, as presented in Table 1. The resulting solutions were heated to 80 °C for 2 hours to facilitate cross-linking, then ultra-sonicated to eliminate air bubbles and homogenize. The gel was frozen and freeze-dried at −80 °C and 10 kPa to produce Cell-A.

4. Preparation of Cell-AP and CA

10 mL of PDMS was dispersed in 25 mL of hexane solvent, followed by an additional 50 µL of DBTL and 3.8 g of TEOS while stirred at 30 °C for 4 hours. Cell-A materials were dipped into the obtained mixture and dried at 90 °C for 12 hours to obtain Cell-AP. Meanwhile, the synthesized Cell-A were pyrolyzed in a tubular furnace at 200 °C for 2 hours in an argon atmosphere. The temperature was then elevated to 700 °C at a heating rate of 5 °C/min and kept for 2 hours to ensure the formation of the aromatic structure, then the samples were cooled to room temperature. The obtained materials were labeled Cell-APX and CA-X (X was based on the ratio of cellulose to PVA), as indicated in Table 1.

5. Characterization

SEM (Hitachi S4800, Japan) was employed to observe the morphology of Cell-A, Cell-AP, and CA. The elemental composition of Cell-AP and CA was analyzed by EDX mapping (Jeol JMS 6490, Japan). Functional groups of the water hyacinth, cellulose, and the prepared materials were identified by FT-IR spectroscopy (Bruker TENSOR-27, Germany) using potassium bromide pellets with various controlling parameters: a wavenumber region of 400-4,000 cm^{-1}, spectrum accuracy of 0.1% T, and resolution of 0.2 cm^{-1}. Diffraction analysis was performed using XRD patterns (Bruker XRD D8, Germany) with operating parameters including a maximum humidity of 70%, a maximum operating temperature of 30 °C, and Cu K_α irradiation (λ_X=0.154 nm) in the range of 0-80° with a scanning speed of 2°/minute. Thermal stability was evaluated by TGA (Thermo Plus TG-8120). Generally, 50 mg of the aerogel was heated from 20 to 700 °C at a rate of 10 °C/min under an N_2 flow of 50 mL/min. The hydrophobicity of Cell-AP and CA was investigated through WCA (DATAPHYSICS OCA-20, Germany) with a magnification of 0.7-4.5 times. The specific surface area and pore size following BET was determined via the adsorption/desorption curves of the nitrogen at 77.35 K and p_0=756 mmHg.

6. Density and Porosity

The mass and dimension of Cell-A, Cell-AP, and CA were measured using a four-digit balance (CPA225D, Germany) and electronic clamp (VOREL-15240 - 150 mm, Germany), respectively. The densities of Cell-A, Cell-AP, and CA were calculated by Eq. (1):

$$\rho = \frac{m}{V} \quad (1)$$

where m (mg) is the weight of the aerogels and V (cm^3) is the corresponding volume obtained by Eq. (2):

$$V = \frac{\pi d^2 h}{4} \quad (2)$$

where d (mm) and h (mm) represent the diameter and height of the aerogels, respectively.

The porosities of Cell-A, Cell-AP, and CA (θ) were determined according to Eq. (3):

$$\theta(\%) = 100 \times \left(1 - \frac{\rho}{\rho_s}\right) \quad (3)$$

where ρ is the density of the aerogels and ρ_s is the density of the solid material.

7. Oil Adsorption Test

The oil adsorption of the Cell-AP and CA materials was investigated using a static model. The samples were placed on the surface of the oil-water mixture for 1 to 10 minutes. After adsorption, the samples were removed and weighed. The oil adsorption capacity was calculated by Eq. (4).

$$Q = \frac{W_s - W_t}{W_t} \quad (4)$$

where Q (mg/g) is the oil adsorption capacity of the samples, W_s (mg) and W_t (mg) are the masses of the sample before and after being tested, accordingly.

To investigate the adsorption behavior of Cell-AP and CA, the adsorption kinetics was compared with two prevalent models, the pseudo-first and pseudo-second-order models, shown in Eqs. (5) and (6), respectively:

$$\ln\left(\frac{Q_m}{Q_m - Q_t}\right) = k_1 t \quad (5)$$

by plotting $\ln\left(\frac{Q_m}{Q_m - Q_t}\right)$ against time, the gradient of the best fit yields a k_1 value.

$$\frac{t}{Q_t} = \frac{1}{k_2 Q_m^2} + \frac{1}{Q_m} t \quad (6)$$

by plotting $\frac{t}{Q_t}$ against time, the gradient of the best gives both $\frac{t}{Q_t}$ and $\frac{1}{k_2 Q_m^2}$, which are then used to determine k_2 by rearranging the equation. Q_t (mg/g) and Q_m (mg/g) are, respectively, the oil adsorption capacity of the aerogel at the investigated time t (minute) and equilibrium. The rate constants k_1 and k_2 were determined from the diagrams for the pseudo-first and pseudo-second-order models.

RESULTS AND DISSCUSION

1. Materials Characterization

The preparation of aerogels from Vietnamese hyacinth is summarized in Fig. 1. The hydrogel was created by hydrogen bonding between the hydroxyl groups of PVA and cellulose (Fig. S1) [11], then freeze-dried to obtain Cell-A. As a result of the freeze-dying process, the ice crystals subsequently removed by sublimation yielded a highly porous structure without structural shrinkage and collapse [2,12,13]. Color changes were additionally observed after surface modification; after being dip-coated in PDMS and pyrolyzed, Cell-A (white) was transformed into Cell-AP (brownish-yellow) and CA (black), respectively.

Fig. 2 shows the SEM images of Cell-A, Cell-AP, and CA. As represented in Fig. 2(a), Cell-A has a layered and stacked structure. Macro- to micropores of various sizes can be seen throughout the surface of the aerogel. In Fig. 2(b), Cell-AP is depicted to have a 3D-network structure. It can be seen that the PDMS coating had no significant effect on the overall porous structure of the mate-

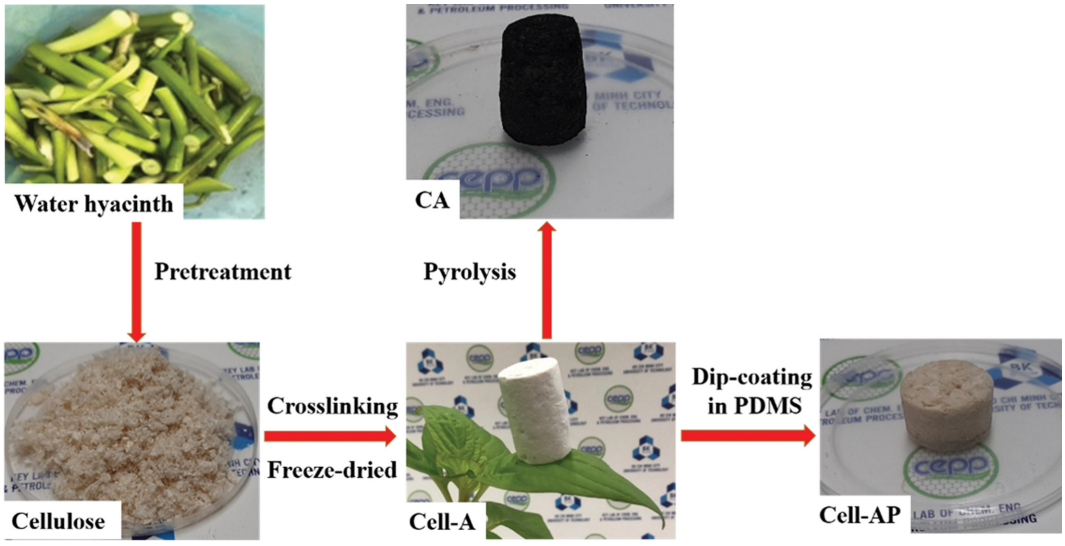

Fig. 1. Fabrication and modification procedure of aerogel materials.

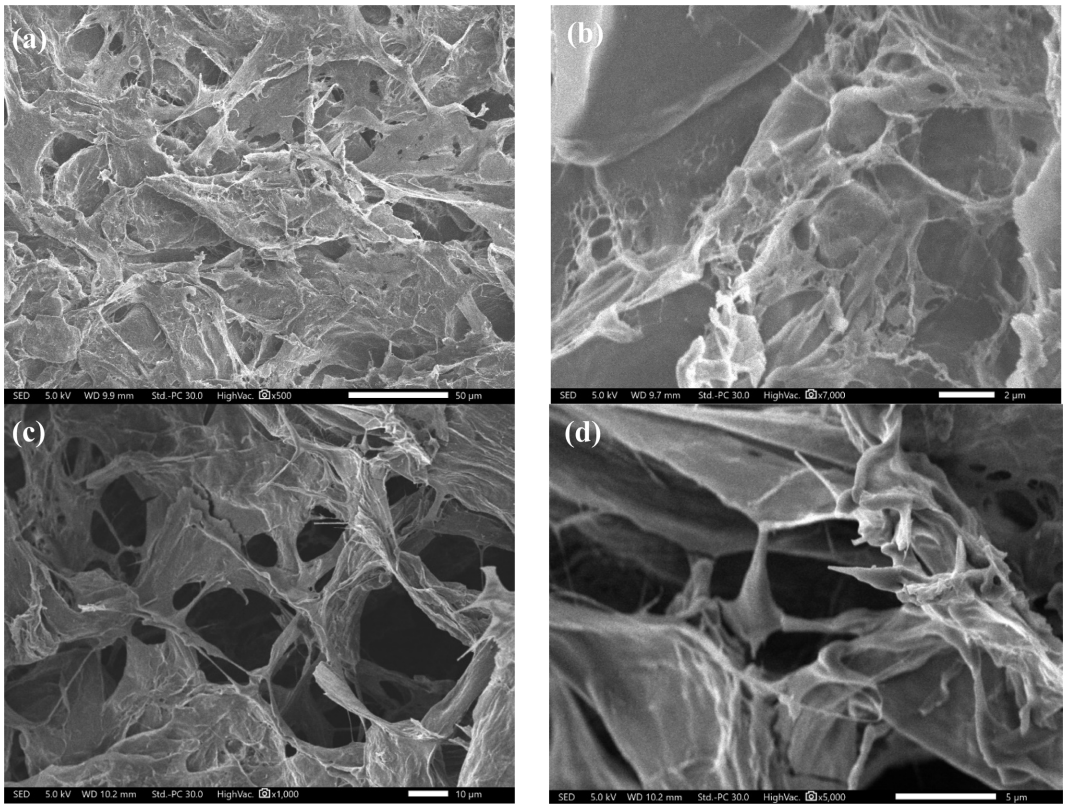

Fig. 2. SEM images of (a) Cell-A, (b) Cell-AP, and (c)-(d) CA.

rial [14]. Fig. 2(c) confirms that the CA was successfully synthesized through pyrolysis without structural breakdown since the cellulose framework from the precursor aerogel managed to inhibit collapse [15]. CA also appears to consist of more meso- and micropores than its precursor, Cell-A. These porous structures provide space for oil storage and facilitate oil entry [15].

The density and porosity of Cell-A, Cell-AP, and CA are displayed in Table S1. All the aerogel samples exhibited high porosity and low density. Density and porosity of Cell-A and Cell-AP showed negligible deviations. It can be explained that the surface modification had little effect on the structure, aside from the additional bonding between the silane groups of PDMS and hydroxyl groups in cellulose [14,16]. In contrast, there is an increase in porosity from Cell-A to CA after pyrolysis because of the reduction of functional chemical groups on the cellulose fiber. As the concentration of cellulose fibers increases, a reduction in porosity and increase in density in the materials could be observed, attributed to the reduction of space of the air pockets between cellulose fibers [17,18]. CA-05 exhibited ultralight density (0.098 g/cm^3) and a superior porosity of 97.483% compared to that of Cell-A05 and Cell-AP05, suggesting that pyrolysis is more efficient for Cell-A modification than dip-coating.

Fig. 3 displays the FTIR spectra of water hyacinth, cellulose, Cell-A, Cell-AP, and CA. Both water hyacinth and cellulose show characteristic peaks at 3,300, 2,910, 1,422, 1,370, 1,138, 1,050, and 895 cm^{-1}, which are typically indicative of cellulose molecules. More specifically, 2,910 and 1,050 cm^{-1} could be resulting from stretching vibration adsorption peak of C-H and glycosidic ring along

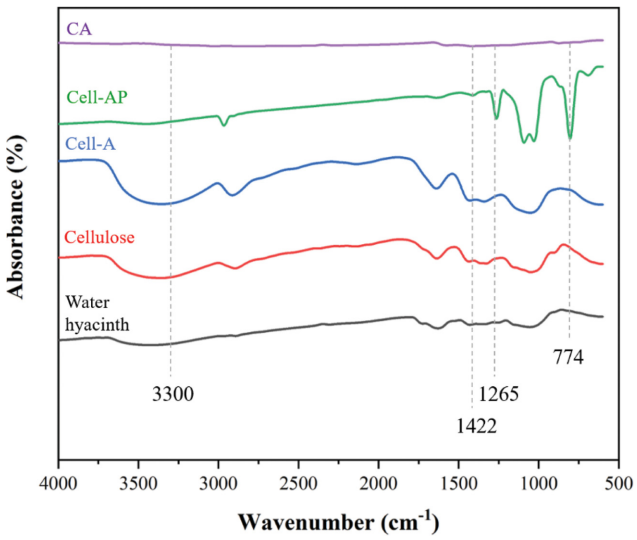

Fig. 3. FTIR spectra of water hyacinth, cellulose, Cell-A, Cell-AP, and CA.

with the side group vibration, respectively [19]. The vibrational peaks at 1,649, 1,590, and 1,505 cm^{-1} are accounted for by the presence of aliphatic esters in lignin and hemicellulose components [20]. Particularly, the peak at 1,649 cm^{-1} might be attributed to the bending vibration peak of O-H [19]. In the spectrum of cellulose, the peak in the region of 1,138-1,164 cm^{-1} is the asymmetric tensile vibration of the C-O-C group of the glycosidic ring [15, 21]. The

peaks of 850 and 2,933 cm^{-1} in the spectrum of Cell-A indicate the presence of -CH_2 bending and C-O stretching vibration of PVA molecules, respectively. While the absorption band at 1,422 cm^{-1} represents C-OH bending, the adsorption band at 1,668 cm^{-1} is attributed to H-O-H bending. Furthermore, the broad peak centered around 3,300 cm^{-1} illustrates the presence of -OH groups [22]. It can be seen from the spectrum of Cell-A that the absorption peaks of cellulose and PVA are present but weakened, an effect of the strong interaction between PVA and cellulose. After surface modification with PDMS, Cell-AP exhibits vibrations at 1,265 and 774 cm^{-1}, which are characteristic of -CH_3 deformation and -Si-C formation, respectively [23]. The intensity of -OH (3,300 cm^{-1}) and C-OH (1,422 cm^{-1}) stretching vibrations is significantly reduced by the replacement of -OH with -O-Si-$(CH_3)_3$ groups (Fig. 3), suggesting an enhancement in hydrophobicity [24]. In the spectrum of CA, the peaks of C-H, C-O, and other functional groups have become weaker or disappeared, indicating that PVA was dehydrogenated by pyrolysis. The O-H groups disappeared and only carbon-containing functional groups remained, which contributes to the hydrophobicity, uniform pore structure, and overall oil absorption of the aerogels [15].

XRD patterns of Cell-A, Cell-AP, and CA are presented in Fig. 4. Cell-A exhibits two characteristic peaks at 2θ=15.8° and 2θ=22.7°, corresponding to the (101) and (200) lattice plane of cellulose [25]. In the XRD pattern of Cell-AP, the substantial reduction of the former characteristic peaks and the emergence of a strong peak at 2θ=14.5° indicates the removal of hydroxyl groups and the introduction of silane groups from PDMS, respectively [14,26]. In comparison to CA, however, the disappearance of 2θ=16.9° and emergence of two broad peaks at 2θ=10.5° and 2θ=25° is observed, while the peak of 2θ=22.7° is weakened. This confirms the generation of amorphous carbon via the carbonization and significant destruction of structural crystals of the cellulose [27], verifying the successful transformation from Cell-A to CA.

EDX analyses of Cell-A and CA are shown in Fig. 5. Carbon and oxygen are naturally assigned to the two oscillating signals with the largest intensities, compared to those of a minority of common elements (below 1%) [28]. CA exhibited a higher peak intensity in carbon composition and a lower peak intensity in oxygen composition, compared to that of Cell-A, further corroborating the carbonization process. The elemental compositions of Cell-A and CA are summarized in Table S2. There is a significant decrease in the elemental ratio of oxygen, while that of carbon increases substantially after the pyrolysis process. The results indicate that Cell-A was successfully carbonized into CA, eliminating oxygen-containing functional groups [29].

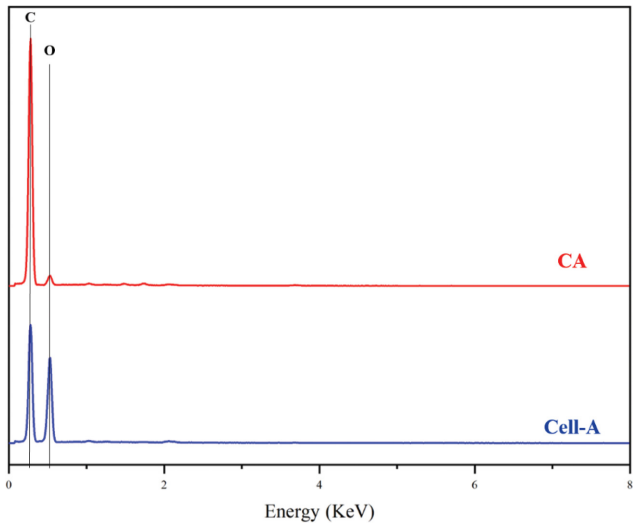

Fig. 5. EDX spectra of Cell-A and CA.

The thermal degradation of Cell-AP and CA was examined from 20 to 800 °C using thermal gravimetric analysis method. The results are shown in Fig. 6; both Cell-AP and CA experienced weight loss at around 30 to 120 °C because of water evaporation [30]. The second weight-loss stage of Cell-AP at around 220 to 315 °C could be attributed to hemicellulose degrading. From 355 to 550 °C, a

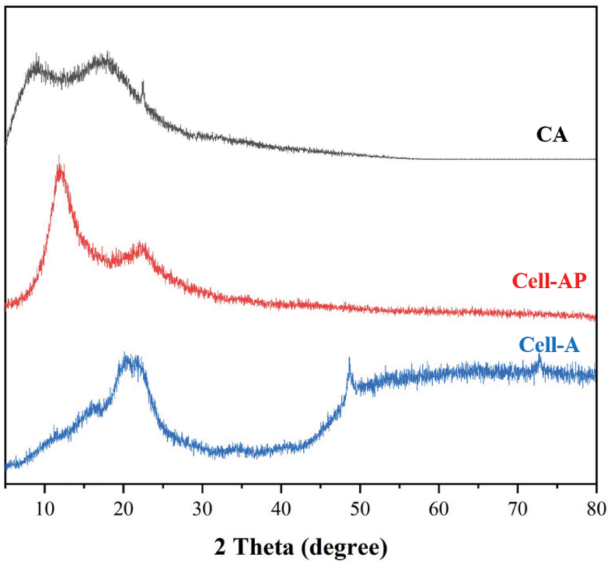

Fig. 4. X-ray diffraction of Cell-A, Cell-AP, and CA.

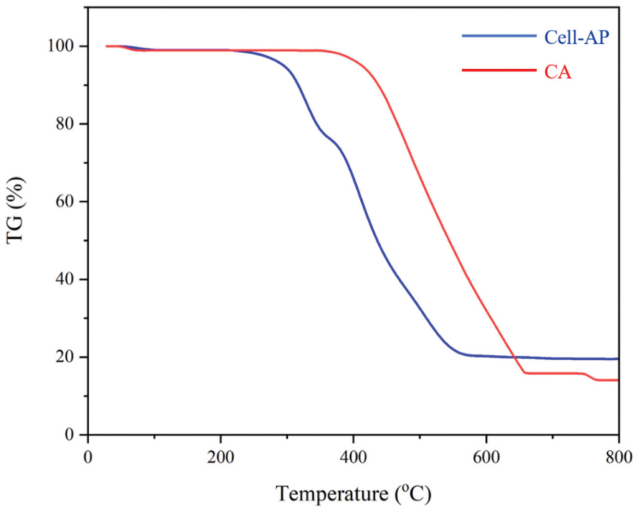

Fig. 6. TGA thermograms of Cell-AP and CA.

massive weight drop in Cell-AP occurred mainly because of the rapid decay of cellulose, which implies the pretreatment steps had removed most of the lignin in the water hyacinth [31]. After most of the weight of the material was reduced, a residue of approximately 19% of the original weight was obtained. The second stage of degradation of CA is around 410 to 660 °C, indicating it is more thermally stable than Cell-AP. It also implies the absence of hemicellulose, cellulose, and lignin because of the complete pyrolysis of Cell-A. The residue of CA, which is approximately 11% of its original weight, is lower than that of Cell-AP. This is likely because of the absence of PDMS in CA.

The nitrogen adsorption/desorption isotherms in Fig. 7 show both Cell-AP and CA exhibit a typical IV isotherm pattern, with a hysteresis loop at high relative pressure [19]. A comparison of specific surface area and average pore size between several materials is presented in Table 2. The difference in specific surface area between Cell-AP (32.71 m^2/g) and CA (63.14 m^2/g) is found to be a result of the pyrolysis process at 700 °C [32]. The average pore size of Cell-AP and CA is 1.63 and 1.59 nm, thereby confirming the formation of micropores (pores of size less than 2 nm), respectively. The appearance of micropores in Cell-AP can be explained by the forming and sublimating of ice crystals at low temperature during the freeze-drying process [2,12,13]. Furthermore, the degradation of cellulose and PVA while pyrolyzing Cell-A leading to the lower of specific surface area and the enhancement of pores size in CA [33].

The WCA is one of the most important standards for assessing oil adsorbents [15]. Fig. S4 shows the hydrophobicity of Cell-A, Cell-AP, and CA. The WCA of Cell-A was 0° (Fig. 8(a)) before modifications; in contrast, the modified aerogels exhibited high hydrophobicity, with water contact angles of 114.3° for Cell-AP and 103.2° for CA (Fig. 8(b) and 8(c)), respectively. The hydrophobicity of the

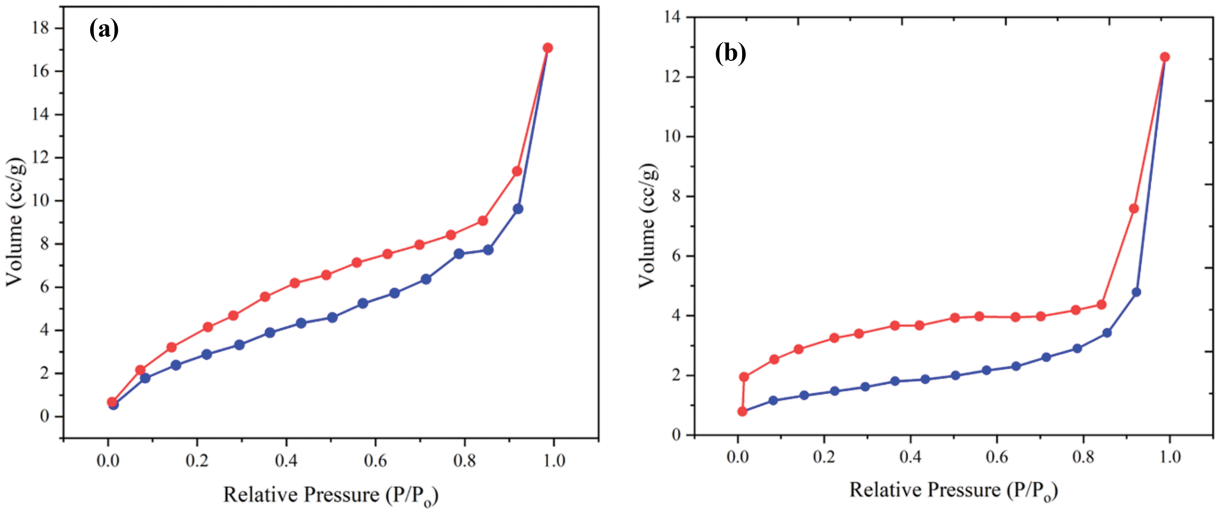

Fig. 7. Nitrogen adsorption-desorption isotherms of (a) Cell-AP and (b) CA.

Table 2. Comparison of specific surface area and average pore size of various materials

Materials	Average pore sizes (nm)	Specific surface areas (m^2/g)	References
Cell-AP	1.59	63.14	This work
CA	1.63	32.71	This work
Cellulose aerogel (paper waste)	11.2	132.26	[34]
Cellulose aerogel (bamboo fibrils)	10	13.42	[35]
Carbon aerogel (bleached softwood kraft pulp fiber)	8.53	69.00	[36]

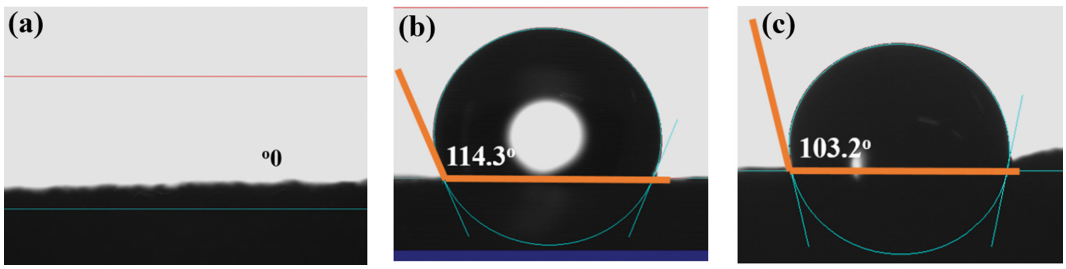

Fig. 8. Water contact angles of (a) Cell-A, (b) Cell-AP, and (c) CA.

modified aerogels was achieved by the replacement of hydroxyl functional groups with silane groups of PDMS or the removal of its hydrophilic groups via pyrolysis [15]. The difference between WCA of Cell-AP and CA was trivial, indicating that the structure did not have any significant effect on the water contact angle [15]. Regarding their lightweight, porous structure, and hydrophobicity, Cell-AP and CA were used to further investigate their oil adsorption capability.

2. Oil Adsorption

Fig. 9 presents the process of adsorbing lubricant oil in a water/oil mixture using Cell-AP and CA. Samples of both Cell-AP and CA with the same height were gently immersed into the heterogeneous oil-water mixture, which then promptly began to adsorb the oil. The oil was successfully adsorbed from the liquid in three minutes for Cell-AP, while it only took CA two minutes under similar conditions. The difference in adsorption time can be explained by the lower density and higher porosity of CA compared to that of Cell-AP [37].

In Fig. 10, both Cell-AP and CA exhibited rapid oil adsorption rates for the first few seconds, then immediately reached saturation after roughly two minutes. The amount of oil CA-15 adsorbed after two minutes is higher (8,106 mg/g) than that of Cell-AP05 (1,570 mg/g). The maximum oil adsorption capacity of CA-15 (Q=8,345 mg/g) is also significantly (4.5 times) greater than that of Cell-AP05 (Q=1,878 mg/g) due to the increase in porosity and decrease in density. For Cell-AP, the oil adsorption capacity decreases with increasing cellulose components because of reducing porosity [18, 38]. The comparison of oil adsorption capacity of Cell-AP and CA with another adsorbent are shown in Table 3. The results show that the oil adsorption capacity of Cell-AP and CA was higher than pyrolyzed banana peel and pyrolyzed rice husk because of the forming porous networks and 3D structure in Cell-AP and CA, leading to higher specific surface area. However, both Cell-AP and CA have lower adsorption capacity than that of cellulose aerogels

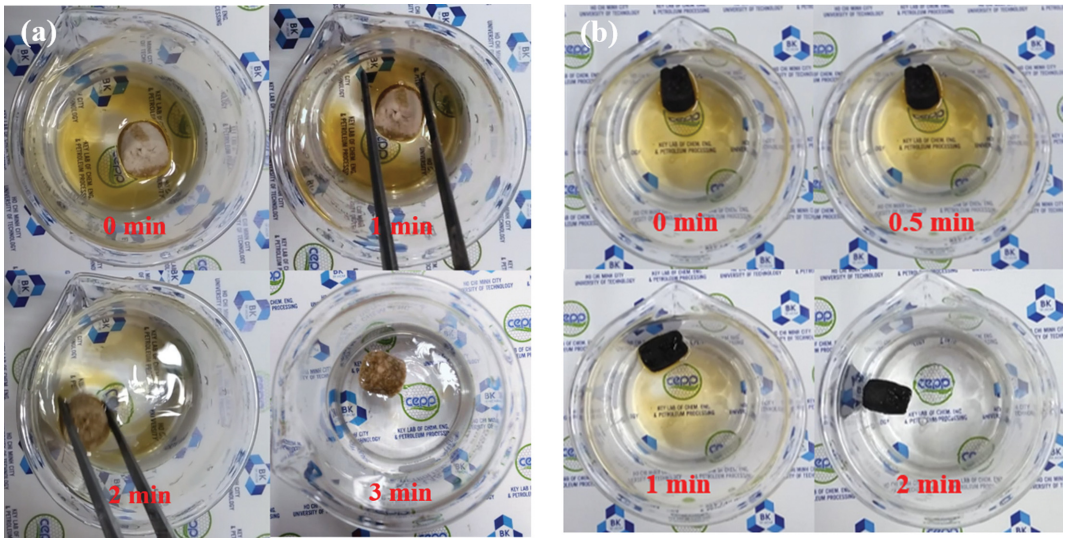

Fig. 9. Adsorption performance of (a) Cell-AP and (b) CA.

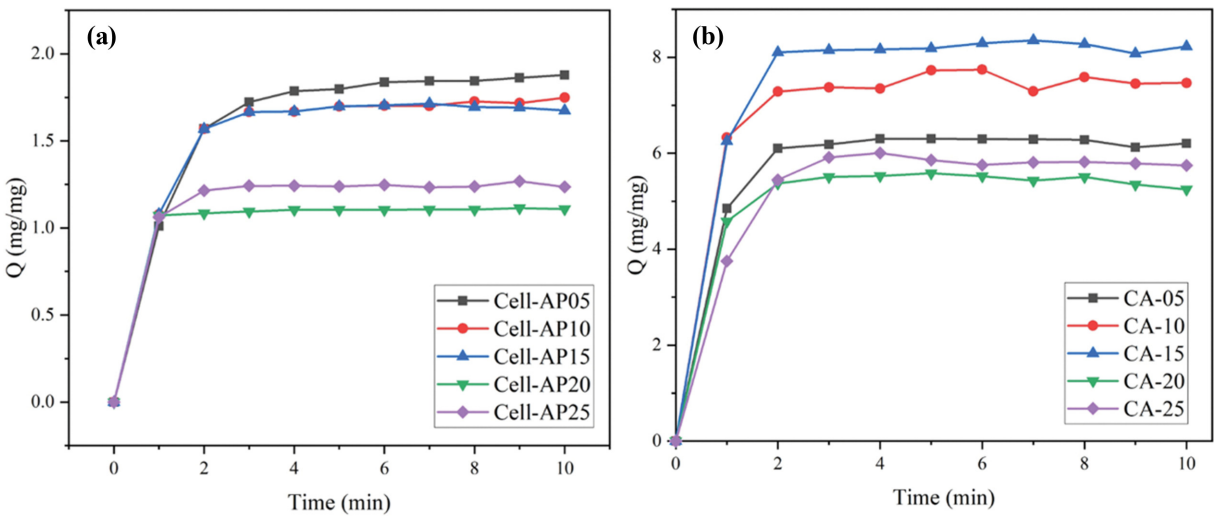

Fig. 10. Adsorption capacity over time of (a) Cell-AP and (b) CA.

Table 3. Comparison of oil adsorption capacity of other materials

Adsorbent	Adsorption capacity (mg/g)	References
Cellulose aerogel (sugarcane bagasse)	25,000	[3]
Cellulose aerogel (pineapple fibers)	37,900	[18]
Pyrolyzed banana peel	500	[39]
Pyrolyzed rice husk	600	[40]
Cellulose aerogel (paper waste)	18,400	[34]
Cell-AP15	1,878	This work
CA-05	8,345	This work

Table 4. Static adsorption results of Cell-AP

Samples		Cell-AP05	Cell-AP10	Cell-AP15	Cell-AP20	Cell-AP25
Q_m (mg/g)		1,845	1,726	1,714	1,106	1,247
First-order	R^2	0.958	0.838	0.941	0.875	0.712
	K_1	0.837	0.501	0.781	0.691	0.811
Second-order	R^2	0.997	0.998	0.997	0.999	0.998
	K_2	0.908	1.451	2.073	18.205	8.367

Table 5. Static adsorption results of CA

Samples		CA-05	CA-10	CA-15	CA-20	CA-25
Q_m (mg/g)		6,301	7,745	8,345	5,385	6,004
First-order	R^2	0.005	0.741	0.752	0.926	0.993
	K_1	2.167	0.898	0.538	0.967	1.623
Second-order	R^2	0.998	0.998	0.998	0.997	0.996
	K_2	1.786	1.557	0.901	3.694	0.823

from sugarcane bagasse and pineapple fibers. This can be explained that the oils chosen to study the adsorption behavior of the aerogels were not the same between these works, leading to the difference of viscosity. More importantly, the oil absorption capacity of Cell-AP and CA shows a clear advantage compared to the oil adsorption capacity of previously reported oil adsorbents, making CA a promising adsorbent material.

3. Oil Adsorption Kinetics

Oil adsorption kinetics are commonly investigated using the pseudo-first-order and pseudo-second-order models; both models were used in this study to analyze the empirical data. The results indicated in Tables 4 and 5 show that the correlation coefficient R^2 of the pseudo-second-order kinetic adsorption model is far greater than that of the pseudo-first-order kinetic adsorption model in both CA and Cell-AP. Therefore, the pseudo-second-order model has higher relative accuracy in predicting both materials' oil adsorption behavior than the pseudo-first model [41]. Additionally, the performance of pseudo-second-order models can be used to investigate the sorption process controlled by chemical adsorption [42].

CONCLUSION

Cell-A was successfully synthesized using water hyacinth by the cross-linking method and freeze-drying process. Cell-A was further modified to obtain hydrophobic Cell-AP and CA with the optimal ratio of cellulose to PVA of 5 : 1 for Cell-AP05 (WCA= 114.3°) and 10 : 1 for CA-15 (WCA=103.2°), respectively. The maximum oil adsorption capacity of CA-15 (Q=8,345 mg/g) was significantly greater than that of Cell-AP05 (Q=1,878 mg/g). The results indicate the optimal fabrication ratio of cellulose to PVA is 5 : 1 and 15 : 1 for Cell-AP and CA, respectively. Furthermore, the pseudo-second-order model is appropriate for predicting the oil absorption behavior of Cell-AP and CA. The synthesized Cell-AP and CA have both shown promise as biomass-derived, eco-friendly materials for future oil adsorption applications.

ACKNOWLEDGEMENTS

We acknowledge the support of time and facilities from Ho Chi Minh City University of Technology (HCMUT), VNU-HCM for this study.

SUPPORTING INFORMATION

Additional information as noted in the text. This information is available via the Internet at http://www.springer.com/chemistry/journal/11814.

REFERENCES

1. I. M. Saadoun, *Impact of oil spills on marine life in Emerging pollutants in the environment-current and further implications*, Intech

Open Publications, Rijeka (2015).
2. L. Y. Long, Y. X. Weng and Y. Z. Wang, *Polymers*, **10**, 623 (2018).
3. Q. B. Thai, S. T. Nguyen, D. K. Ho, T. D. Tran, D. M. Huynh, N. H. N. Do, T. P. Luu, P. K. Le, D. K. Le, N. P. Thien and D. M. Hai, *Carbohydrate*, **228**, 115365 (2020).
4. J. Wei, S. H. Gui, J. H. Wu, D. D. Xu, Y. Sun, X. Y. Dong and Y. F. Li, *Appl. Environ. Biotechnol.*, **4**, 11 (2019).
5. N. V. Dao and V. H. Van, *Rev. Argentina de Clin. Psicol*, **29**, 202 (2020).
6. A. M. L. PN and G. Madhu, *Int. J. Urban Sustain. Dev.*, **1**, 48 (2011).
7. M. H. Julien, M. W. Griffiths and J. N. Stanley, *ACIAR Monograph*, **435**, 33682 (2001).
8. Y. L. Ding, Z. Tian, H. J. Li and X. M. N. Wang, *Carbon*, **34**, 315 (2019).
9. L. E. Nita, A. Ghilan, A. G. Rusu, I. Neamtu and A. P. Chiriac, *Pharmaceutics*, **12**, 449 (2020).
10. Q. Zheng, Z. Cai and S. Gong, *J. M. Chem. A.*, **2**, 3110 (2014).
11. M. E. Achaby, N. E. Miri, A. Aboulkas, M. Zahouily, E. Bilal, A. Barakat and A. Solhy, *Int. J. Biol. Macromol.*, **96**, 340 (2017).
12. I. Khan, A. Elhissi, M. Shah, M. A Alhnan and W. Ahmed, *Biomaterials and medical tribology*, Elsevier Publications, Amsterdam (2013).
13. W. Surapolchai and D. A. Schiraldi, *Polym. Bull.*, **65**, 951 (2010).
14. C. Cao, M. Ge, J. Huang, S. Li, S. Deng, S. Zhang, Z. Chen, K. Zhang, S. S. A. Deyab and Y. Lai, *J. M. Chem. A*, **4**, 12179 (2016).
15. L. Zhou and Z. Xu, *J. Hazard. M.*, **388**, 121804 (2020).
16. M. Abdelmouleh, S. Boufi, A. ben Salah, M. N. Belgacem and A. Gandini, *Langmuir*, **18**, 3203 (2002).
17. U. G. T. M. Sampath, Y. C. Ching, C. H. Chuah, J. J. Sabariah and P-C. Lin, *Materials*, **9**, 991 (2016).
18. N. H. N. Do, T. P. Luu, Q. B. Thai, L. K. Duyen, D. N. Q. Chau, S. T. Nguyen, P. K. Le, N. P. Thien and H. M. Duong, *M. Chem. Phy.*, **242**, 122267 (2020).
19. H. Zhuo, Y. Hu, Z. Chen and L. Zhong, *Carbohydr. Polym.*, **215**, 322 (2019).
20. L. Liu, Z. Y. Gao, X. P. Su, X. Chen, L. Jiang and J. M. Yao, *ACS Sustain. Chem. Eng.*, **3**, 432 (2015).
21. D. Trache, M. H. Hussin, C. T. H. Chuin, S. Sabar, M. R. N. Fazita, O. F. A. Taiwo, T. M. Hassan and M. K. M. Haafiz, *Int. J. Biol. Macromol.*, **93**, 789 (2016).
22. L. Zhu, Y. Wang, Y. Wang, L. You, X. Shen and S. Li, *Micropor. Mesopor. Mater.*, **241**, 285 (2017).
23. S. Li, S. Zhang and X. Wang, *Langmuir*, **24**, 5585 (2008).
24. S. Xiao, R. Gao, Y. Lu, J. Li and Q. Sun, *Carbohydr. Polym.*, **119**, 202 (2015).
25. Z. Li, L. Zhong, T. Zhang, F. Qiu, X. Yue and D. Yang, *ACS Sustain. Chem. Eng.*, **7**, 9984 (2019).
26. L. Wang, J. Feng, Y. Jiang, L. Li and J. Feng, *RSC Adv.*, **9**, 10948 (2019).
27. L. Segal, J. J. Creely, A. E. Martin, Jr. and C. M. Conrad, *Textile Res. J.*, **20**, 786 (1959).
28. K. Srasri, M. Thongroj, P. Chaijiraaree, S. Thiangtham, H. Manuspiya, P. Pisitsak and S. Ummartyotin, *Int. J. Biol. Macromol.*, **119**, 662 (2018).
29. S. Geng, J. Wei, S. Jonasson, J. Hedlund and K. Oksman, *ACS Appl. Mater. Interfaces*, **12**, 7432 (2020).
30. E. Uitterhaegen, Q. H. Nguyen, O. Merah, C. V. Stevens, T. Talou, L. Rigal and P. Evon, *J. Renew. M.*, **4**, 225 (2016).
31. H. Zhuo, Y. Hu, Z. Chen, X. Peng, H. Lai, L. Liu, Q. Liu, C. Liu and L. Zhong, *ACS Sustain. Chem. Eng.*, **8**, 11921 (2020).
32. D. Angın and S. Şensöz, *Int. J. Phytoremediation*, **16**, 684 (2014).
33. W. Li, G. Reichenauer and J. Fricke, *Carbon*, **40**, 2955 (2002).
34. S. T. Nguyen, J. Feng, N. T. Le, A. T. T. Le, N. Hoang, V. B. C. Tan and H. M. Duong, *In. Eng. Chem. Res.*, **52**, 18386 (2013).
35. D. D. Nguyen, C. M. Vu, H. T. Vu and H. J. Choi, *Materials*, **12**, 1407 (2019).
36. E. Lei, W. Li, C. Ma and S. Liu, *Mater. Chem. Phys.*, **214**, 291 (2018).
37. H. D Jonge and M. C. Mittelmeijer-Hazeleger, *Environ. Sci. Technol.*, **30**, 408 (1996).
38. N. H. N. Do, T. P. Luu, Q. B. Thai, L. K. Duyen, D. N. Q. Chau and S. T. Nguyen, *Mater Technol.*, **35**, 807 (2020).
39. S. S. Lam, R. K. Liew, C. K. Cheng, N. Rasit, C. K. Ooi, N. L. Ma, N. J. Han, W. H. Lam, C. T. Chong and H. A. Chase, *J. Environ. Manage.*, **213**, 400 (2018).
40. S. Kumagai, Y. Noguchoi, Y. Kurimoto and K. Takeda, *Waste Manage.*, **27**, 554 (2007).
41. J. Feng, S. T. Nguyen, Z. Fan and H. M. Duong, *Chem. Eng. J.*, **270**, 168 (2015).
42. A. M. M. Vargas, A. L. Cazetta, M. H. Kunita, T. L. Silva and V. C. Almeida, *Chem. Eng. J.*, **168**, 722 (2011).

Supporting Information

Fabrication and modification of cellulose aerogels from Vietnamese water hyacinth for oil adsorption application

La Nam Phat[*,], Tran Quoc Thang[***], Huynh Cam Nguyen[*,**], Dang Thi My Duyen[*,**], Dao Xuan Tien[***], Bui Dang Dang Khoa[*,**], Pham Tan Khang[*,**], Nguyen Thi Huong Giang[*,**], Hoang Minh Nam[*,**,****], Mai Thanh Phong[*,**,****], and Nguyen Huu Hieu[*,**,****,†]**

*VNU-HCM, Key Laboratory of Chemical Engineering and Petroleum Processing (Key CEPP Lab), Ho Chi Minh City University of Technology (HCMUT), 268 Ly Thuong Kiet Street, District 10, Ho Chi Minh City, Vietnam
**Faculty of Chemical Engineering, Ho Chi Minh City University of Technology (HCMUT), 268 Ly Thuong Kiet Street, District 10, Ho Chi Minh City, Vietnam
***Faculty of Chemistry Ho Chi Minh City University of Science (HCMUS), 227 Nguyen Van Cu Street, District 5, Ho Chi Minh City, Vietnam
****Vietnam National University Ho Chi Minh City, Linh Trung Ward, Thu Duc District, Ho Chi Minh City, Vietnam
(*Received 24 March 2021 • Revised 15 May 2021 • Accepted 20 May 2021*)

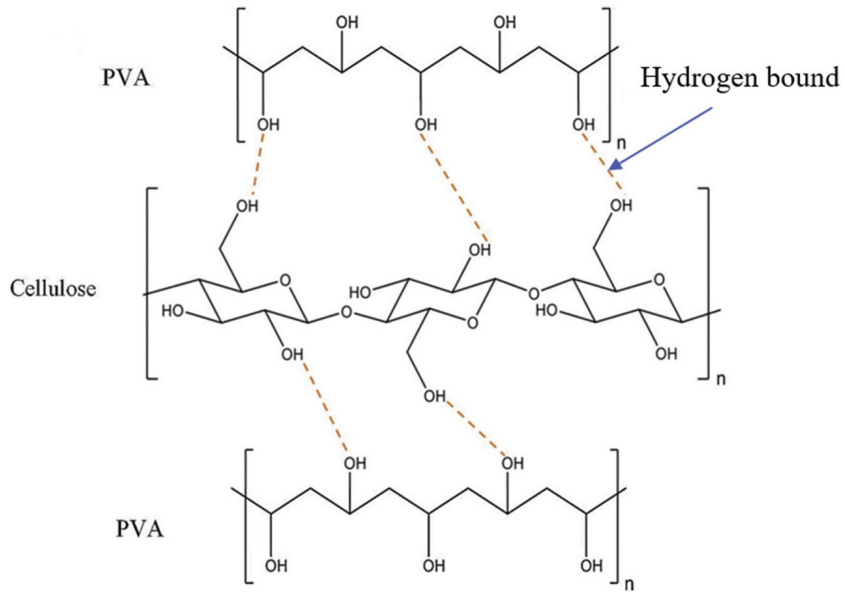

Fig. S1. Cross-linking mechanism between cellulose and PVA in Cell-A.

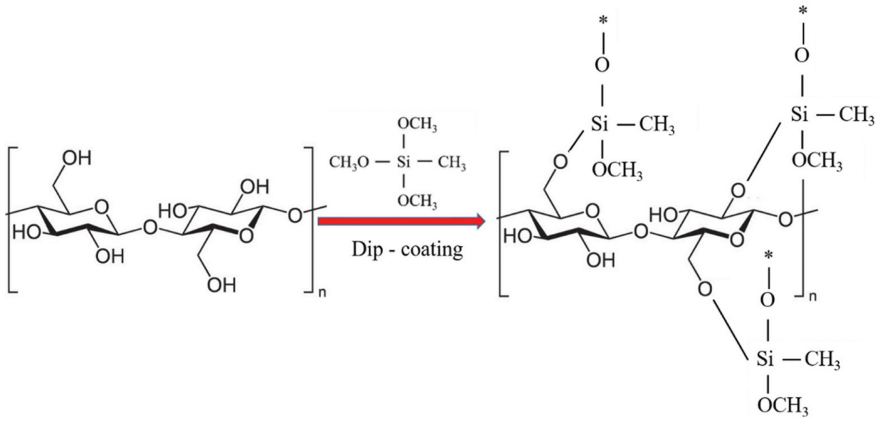

Fig. S2. Proposed mechanism of surface modification process with PDMS.

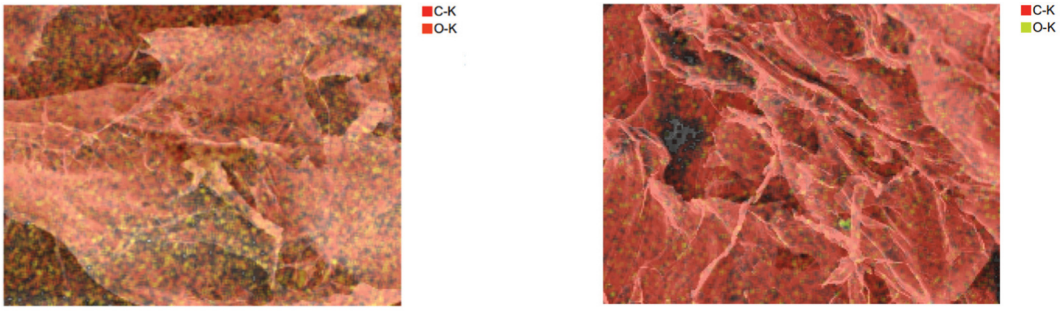

(a) (b)

Fig. S3. Mapping elements on (a) Cell-A and (b) CA.

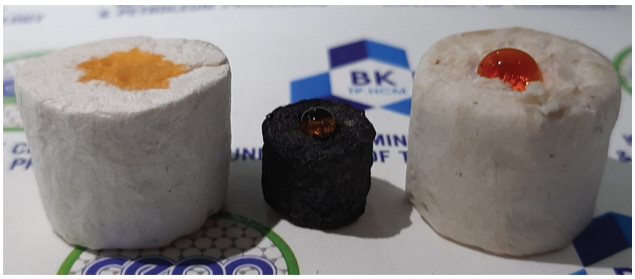

Fig. S4. Hydrophobicity of Cell-A, CA, and Cell-AP.

Table S1. Densities and porosities of Cell-A, Cell-AP, and CA

	Samples	Density (g/cm^3)	Porosity (%)
Cell-A	Cell-A05	0.121	88.126
	Cell-A10	0.131	87.306
	Cell-A15	0.135	86.828
	Cell-A20	0.213	79.351
	Cell-A25	0.232	77.440
Cell-AP	Cell-AP05	0.121	88.126
	Cell-AP10	0.131	87.306
	Cell-AP15	0.136	86.826
	Cell-AP20	0.214	79.350
	Cell-AP25	0.232	77.442
CA	CA-05	0.098	97.483
	CA-10	0.102	95.604
	CA-15	0.156	94.372
	CA-20	0.193	92.765
	CA-25	0.204	91.324

Table S2. Elemental composition of Cell-A and CA

Element ratio (%)	Cell-A	CA
C	55.98±0.10	93.41±0.11
O	43.53±0.16	6.59±0.09